

# Ultrafast carrier reservoir semiconductor optical amplifiers-based all-optical AND logic gate

Amer Kotb<sup>a,b,\*</sup>

<sup>a</sup>Chinese Academy of Sciences, Changchun Institute of Optics, Fine Mechanics, and Physics, GPL, State Key Laboratory of Applied Optics, Changchun, China

<sup>b</sup>University of Fayoum, Department of Physics, Faculty of Science, Fayoum, Egypt

**Abstract.** It has become an imperative reality to find an alternative for the conventional bulk semiconductor optical amplifier (SOA), which suffers from the slow dynamic response, in light of the increased need for higher speeds. In this research, the carrier reservoir SOA (CR-SOA) is employed as a suitable alternative to investigate the all-optical AND logic gate for the first time at an operating speed of 100 Gb/s. For the reliability of the results, the CR-SOAs- and the conventional SOAs-based Mach–Zehnder interferometer are compared in the same operating conditions that include the effects of the amplified spontaneous emission noise and the operating temperature to obtain more realistic simulation results. The results of Wolfram Mathematica proved that the considered Boolean function is executed at 100 Gb/s with a higher quality factor when using CR-SOAs compared to SOAs, i.e., 14 versus 4.7. © 2021 Society of Photo-Optical Instrumentation Engineers (SPIE) [DOI: [10.1117/1.OE.60.2.026104](https://doi.org/10.1117/1.OE.60.2.026104)]

**Keywords:** all-optical AND logic gate; carrier reservoir semiconductor optical amplifier; Mach–Zehnder interferometer.

Paper 20201316 received Nov. 2, 2020; accepted for publication Jan. 29, 2021; published online Feb. 19, 2021.

## 1 Introduction

Over the past few decades, the use of data rates has become greater than ever. The performance of the optical networks with the largest capacity suffers from many problems that can be overcome by optical signal processing. Optical processing provides more capacity with ultrahigh speed without the need to convert from optical to electrical or vice versa. On the other hand, optical gates are the main element to perform optical processing. Many optical devices were used to realize the optical gate and the most prominent of which was the semiconductor optical amplifier (SOA). Unfortunately, the slow gain recovery time of the SOA has stood in the way of its use at higher data rates.<sup>1</sup> There were many solutions to overcome this obstacle, perhaps the most prominent being the addition of quantum dots (QDs), which provides a faster response, in the active region (AR) layer of the SOA, but unfortunately, it is very difficult to fabricate uniform QDs.<sup>2</sup> For this, it was necessary to search for an alternative that works at faster rates and is easy and cheap. The carrier reservoir SOA (CR-SOA) is considered the most suitable to override the limitations of the (QD) SOA devices. The CR-SOA provides a layer that carries the necessary backup carriers in the case of a depletion of the AR, as is the case with the wetting layer in the QD-SOA.<sup>3</sup> The CR layer is located close to the AR layer as shown in the band diagram of the CR-SOA of Fig. 1. The ultrafast transition, which does not exceed a few picoseconds, from the CR to the AR can speed up the dynamic response of the conventional bulk SOA and thus it can work at higher rates. For this, the CR-SOA-assisted Mach–Zehnder interferometer (MZI) is used for the first time to analyze the logic gate AND at 100 Gb/s. MZI has attracted attention during the past years as a suitable candidate in designing logic gates due to its unique characteristics such as small size and low energy consumption in addition to the practicability.<sup>4</sup> So far, the performance of all-optical AND logic gate is investigated using conventional bulk SOAs at different data rates not more than 80 Gb/s.<sup>4–9</sup> To demonstrate the superiority of the CR-SOA,

---

\*Address all correspondence to Amer Kotb, [amer@ciomp.ac.cn](mailto:amer@ciomp.ac.cn)

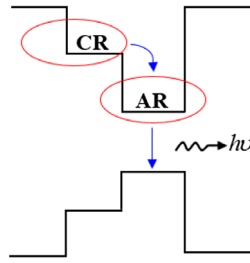


Fig. 1 CR-SOA band diagram.

a comparison was made between it and the conventional bulk SOA under the same operating conditions, including the effects of the amplified spontaneous emission (ASE) noise and operating temperature. The quality factor (QF) metric was used to evaluate the performance of the considered logic gate.

## 2 AND Logic Gate at 100 Gb/s

The AND logic gate gives “1” output when only all of its inputs are 1. The diagram and truth table of the AND logic gate using CR-SOAs-assisted MZI are schematically shown in Fig. 2.

We note the use of only two input light sources to perform the AND logic gate, which works to reduce the cost of establishing this scheme in practice.<sup>4</sup> As in Fig. 2, signal A is injected into CR-SOA1 via wavelength-selective coupler (WSC) while signal B is divided into two halves by the 3-dB optical coupler (OC) to then enter into both CR-SOA1 and CR-SOA2 from the middle port of the MZI. Signal A induces the phase change of signal B via cross-phase modulation in CR-SOAs. Accordingly, when the value of signal A is “0,” there is no phase change induced on signal B and therefore the result is 0. When A is 1 and B is 0, then it results in 0 output simply because there is no input signal to mark the required perturbation in the balanced CR-SOAs-MZI. And when the value of both A and B is 1 where only then the output signals interfere constructively to give “1” output. By this behavior, the AND logic gate is functionally achieved according to its truth table attached in Fig. 2.

For the first time, the following nonlinear rate equations of the CR-SOA, including both interband and intraband nonlinear effects, are employed in the study of the performance of the AND logic gate, i.e., Refs. 1 and 2:

$$\frac{dh_{AR}(t)}{dt} = \frac{h_{CR}(t) - h_{AR}(t)}{\tau_i(1 + \eta)} + \frac{\eta h_0}{\tau_c(1 + \eta)} - \frac{h_{AR}(t)}{\tau_c} - (\exp[h_{AR}(t) + h_{CH}(t) + h_{SHB}(t)] - 1) \frac{P_{in}(t)}{E_{sat}}, \quad (1)$$

$$\frac{dh_{CR}(t)}{dt} = -\frac{\eta(h_{CR}(t) - h_{AR}(t))}{\tau_i(1 + \eta)} + \frac{h_0 - h_{CR}(t)}{\tau_c(1 + \eta)} - \frac{h_{CR}(t)}{\tau_c}, \quad (2)$$

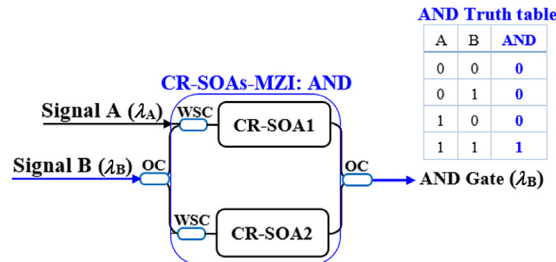


Fig. 2 AND schematic diagram and corresponding truth table using CR-SOAs-MZI. OC: 3-dB optical coupler. WSC: wavelength-selective coupler.

$$\frac{dh_{CH}(t)}{dt} = -\frac{h_{CH}(t)}{\tau_{CH}} - \frac{\varepsilon_{CH}}{\tau_{CH}} (\exp[h_{AR}(t) + h_{CH}(t) + h_{SHB}(t)] - 1)P_{in}(t), \quad (3)$$

$$\frac{dh_{SHB}(t)}{dt} = -\frac{h_{SHB}(t)}{\tau_{SHB}} - \frac{\varepsilon_{SHB}}{\tau_{SHB}} (\exp[h_{AR}(t) + h_{CH}(t) + h_{SHB}(t)] - 1)P_{in}(t) - \frac{dh_{AR}(t)}{dt} - \frac{dh_{CH}(t)}{dt}, \quad (4)$$

where  $h_{AR}$ ,  $h_{CR}$ ,  $h_{CH}$ , and  $h_{SHB}$  are the CR-SOAs gain integrated over its length for the carrier recombination between AR and CR region, carrier heating (CH), and spectral hole burning (SHB).  $\tau_i$  is the transition time from CR to AR and  $\tau_c$  is the carrier lifetime in both AR and CR.  $\eta$  denotes the population inversion factor given by  $\eta = N_{AR}/N_{CR}$ , where  $N_{AR}$  and  $N_{CR}$  are, respectively, the carrier density in AR and CR.  $h_0 = \log[G_0]$ , where  $G_0$  is the unsaturated power gain given by  $G_0 = a\Gamma(I\tau_c/eV - N_{tr})L$ ,<sup>1</sup> where  $a$  is the differential gain,  $\Gamma$  is the optical confinement factor,  $I$  is the injection bias current,  $e$  is the electron charge,  $V$  is the AR volume,  $N_{tr}$  is the transparency carrier density, and  $L$  is the AR length.  $E_{sat}$  is the saturation energy expressed by  $E_{sat} = P_{sat}\tau_c = wd\hbar\omega_0/a\Gamma$ ,<sup>1</sup> where  $P_{sat}$  is the saturation energy,  $w$  and  $d$  are the width and thickness of the AR, respectively,  $\hbar$  is the reduced Planck's constant (i.e.,  $h/2\pi$ ), and  $\omega_0$  is the central frequency.  $\tau_{CH}$  and  $\tau_{SHB}$  are the temperature relaxation rates due to CH and SHB, respectively.  $\varepsilon_{CH}$  and  $\varepsilon_{SHB}$  are the nonlinear gain suppression factors due to CH and SHB, respectively.

The gain resulting from each CR-SOA is then given by the following relationship:<sup>1,4</sup>

$$G_{CR-SOA_i}(t) = \exp[h_{AR}(t) + h_{CH}(t) + h_{SHB}(t)], \quad i = 1, 2 \quad (5)$$

The phase change on the probe wave resulting from each CR-SOA is given as<sup>1,4</sup>

$$\Phi_{CR-SOA_i}(t) = -0.5(\alpha h_{AR}(t) + \alpha_{CH} h_{CH}(t)), \quad i = 1, 2 \quad (6)$$

where  $\alpha$  is the traditional linewidth enhancement factor, namely,  $\alpha$ -factor, and  $\alpha_{CH}$  is the CH linewidth enhancement factor. The  $\alpha_{SHB}$  contribution is zero as noted in Eq. (6), i.e.,  $\alpha_{SHB} = 0$ .<sup>4</sup>

The gate AND has been accomplished with more than acceptable performance using only two input laser sources, one for A and the other for B. The input powers entered, as shown in Fig. 2, in CR-SOA1 and CR-SOA2, are, respectively, expressed as<sup>4</sup>

$$P_{in,CR-SOA_1}(t) = P_A(t) + 0.5P_B, \quad (7)$$

$$P_{in,CR-SOA_2}(t) = 0.5P_B(t), \quad (8)$$

where those pulses  $A$  and  $B$  are assumed to be return-to-zero Gaussian input pulses, which are widely used in optical networks as a result of their distinctive properties, i.e., Ref. 1:

$$P_{A,B}(t) \equiv P_{in}(t) = \sum_{n=1}^N \alpha_{n(A,B)} \frac{2\sqrt{\ln[2]}E_0}{\sqrt{\pi}\tau_{FWHM}} \exp\left[-\frac{4\ln[2](t-nT)^2}{\tau_{FWHM}^2}\right] \quad (9)$$

where  $\alpha_{n(A,B)}$  is the  $n$ 'th pulse of streams A and B, i.e.,  $\alpha_{n(A,B)} = 1$  or 0.  $E_0$  is the input pulse energy,  $\tau_{FWHM}$  is the pulse width [i.e., full-width at half maximum (FWHM)],  $N = 2^7 - 1$ <sup>4</sup> is the length of the pseudorandom binary sequence (PRBS), namely, PRBS-7, and  $T$  is the bit period, which is the inverse of the operating data rate.

At the CR-SOAs-MZI output port, the logic gate AND is performed from the total gains (i.e.,  $G_{CR-SOA_{1,2}}(t)$ ) and phase changes (i.e.,  $\Phi_{CR-SOA_{1,2}}(t)$ ) of the CR-SOA1 and CR-SOA2, i.e., Ref. 4:

$$P_{AND}(t) = 0.25P_B(t) \left( \frac{G_{CR-SOA_1}(t) + G_{CR-SOA_2}(t) - 2\sqrt{G_{CR-SOA_1}(t)G_{CR-SOA_2}(t)}}{\cos[\Phi_{CR-SOA_1}(t) - \Phi_{CR-SOA_2}(t)]} \right). \quad (10)$$

The QF is considered to be one of the most sensitive tools in performance evaluation. This metric is defined as  $QF = (P_1 - P_0)/(\sigma_1 + \sigma_0)$ ,<sup>1</sup> where  $P_1$  and  $P_0$  are the mean peak powers of

**Table 1** AND default parameters.<sup>1–10</sup>

Symbol	Definition	Value	Unit
$E_0$	Pulse energy	0.1	pJ
$\tau_{\text{FWHM}}$	Pulse width	1	ps
$T$	Bit period	10	ps
$N$	PRBS length	127	—
$\lambda_A$	Wavelength of data A	1555	nm
$\lambda_B$	Wavelength of data B	1550	nm
$I$	Injection current	200	mA
$P_{\text{sat}}$	Saturation power	30	mW
$\tau_c$	Carrier lifetime	200	ps
$\tau_t$	Transition lifetime from CR to AR	5	ps
$\eta$	Population inversion factor	0.3	—
$\alpha$	$\alpha$ -factor	5	—
$\alpha_{\text{CH}}$	CH linewidth enhancement factor	1	ns
$\alpha_{\text{SHB}}$	SHB linewidth enhancement factor	0	ns
$\epsilon_{\text{CH}}$	CH nonlinear gain suppression factor	0.2	$\text{W}^{-1}$
$\epsilon_{\text{SHB}}$	SHB nonlinear gain suppression factor	0.2	$\text{W}^{-1}$
$\tau_{\text{CH}}$	Temperature relaxation rate	0.3	ps
$\tau_{\text{SHB}}$	Carrier–carrier scattering rate	0.1	ps
$\Gamma$	Confinement factor	0.3	—
$a$	Differential gain	$10^{-16}$	$\text{cm}^2$
$N_{\text{tr}}$	Transparency carrier density	$10^{18}$	$\text{cm}^{-3}$
$L$	Length of AR	0.5	mm
$d$	Thickness of AR	0.3	$\mu\text{m}$
$w$	Width of AR	3	$\mu\text{m}$
$G_0$	Unsaturated power gain	30	dB
$N_{\text{SP}}$	Spontaneous emission factor	2	—
$\nu$	Optical frequency	193.55	THz
$B_0$	Optical bandwidth	2	nm
$\hbar$	Reduced Planck's constant	$1.05 \times 10^{-34}$	Js

1 and 0 bits, respectively, whereas  $\sigma_1$  and  $\sigma_0$  are the corresponding standard deviations. The value of the QF must exceed six for an acceptable performance<sup>1,4</sup> to keep the value of the related bit-error-rate  $<10^{-9}$ .<sup>10</sup> The time-dependent equations mentioned above Eqs. (1)–(10) are solved using Adams numerical method of Wolfram Mathematica. The default parameters used herein are cited in Table 1.<sup>1–10</sup> These values are used for both CR-SOA and conventional bulk SOA to make a fair comparison.

The comparison of Figs. 3 and 4 shows the advantage of CR-SOA in design AND logic gate with achieving a high QF value of 14 compared to a value of 4.7 when using SOA. The ultrafast

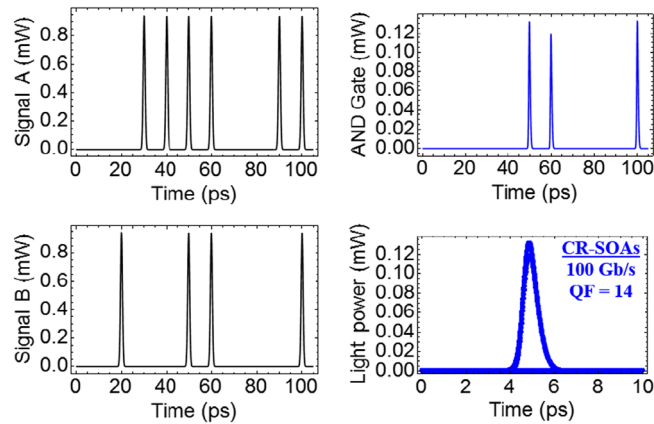


**Fig. 3** AND numerical results using CR-SOAs-MZI at 100 Gb/s with 14 QF.

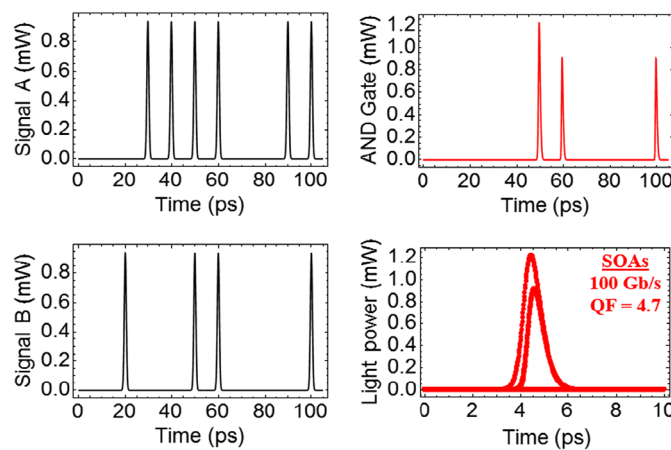


**Fig. 4** AND numerical results using SOAs-MZI at 100 Gb/s with 4.7 QF.

transition from the CR layer to the CR layer resulted in this high QF value while the slow recovery time in bulk SOA caused his inability to realize the AND logic gate at 100 Gb/s with acceptable quality value.

We cannot neglect the importance of both transition time from the CR layer to the AR layer ( $\tau_t$ ) and the population inversion factor ( $\eta$ ) in the performance of the considered logic gate. Therefore, their effects on the performance of the AND logic gate are examined as shown in Fig. 5. In the event of the depletion of the carriers from the AR with increased input signal power, then the CR transports the charges to the AR in a very short time that does not exceed a few picoseconds. Therefore, for a shorter  $\tau_t$ , the transition from CR to AR is rapid, resulting in faster recovery, and hence the value of the QF is increased as shown in Fig. 5(a). On the other hand,  $\eta$  controls the amount of the carrier density in both the AR and the CR, i.e.,  $\eta = N_{AR}/N_{CR}$ . Thus, if  $\eta$  is small, meaning the CR population is high, the gain recovery time becomes faster, resulting in higher quality value [Fig. 5(b)].

In the following results, we compare between CR-SOAs- and SOAs-based AND logic gate through studying the dependence of the QF on ASE noise, operating temperature, data rate, and PRBS length. The ASE power is numerically added to the AND output power of Eq. (13) using  $P_{ASE} = N_{SP}(G_0 - 1)2\pi\hbar\nu B_0$ .<sup>11</sup> The effect of the operating temperature is considered as a quasi-Fermi energy level of the carrier density in CR and AR layers.<sup>2</sup> These parameters greatly affect the performance of both amplifiers, but we note that the CR-SOA resists these effects and still gives an acceptable performance even at higher values of these parameters. The CR-SOA stands up to achieve an acceptable performance even at 4  $\mu$ W of ASE with 6.2 QF [Fig. 6(a)], 330 K of operating temperature with 6.5 QF [Fig. 6(b)], 160 Gb/s of data rate with 6.1 QF

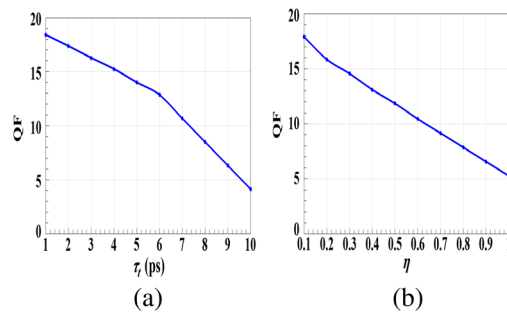


**Fig. 5** AND QF using CR-SOAs-MZI at 100 Gb/s versus (a) transition time from CR to AR ( $\tau_t$ ) and (b) population inversion factor ( $\eta$ ).

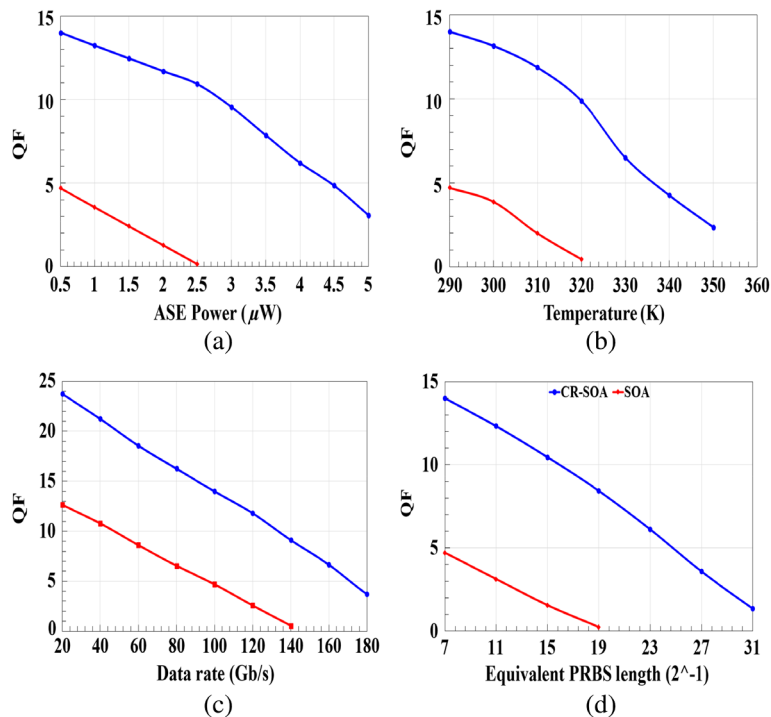


**Fig. 6** AND QF for CR-SOAs- and SOAs-based MZI versus (a) ASE power; (b) operating temperature; (c) data rate; and (d) equivalent PRBS length.

[Fig. 6(c)], and up to  $2^{23} - 1$  of PRBS with 6.2 QF [Fig. 6(d)], whereas, these results are impossible to achieve when using conventional bulk SOA.

### 3 Conclusion

Carrier reservoir semiconductor optical amplifier (CR-SOA) was used for the first time in the study of the all-optical AND logic gate at 100 Gb/s. The CR-SOA achieved more acceptable results compared to conventional bulk SOA when examining the effects of the critical parameters on the output QF. We believe that the CR-SOA will have an important role in designing ultrafast logic gate circuits.

### Acknowledgments

Amer Kotb thanks the CAS's President's International Fellowship Initiative (Grant No. 2019FYT0002) and the Talented Young Scientist Program of the Chinese Academy of Sciences for supporting this work. The author reports no conflicts of interest.

## References

1. N. K. Dutta and Q. Wang, *Semiconductor Optical Amplifiers*, 2nd ed., World Scientific, Singapore (2013).
2. H. Sun et al., "Gain dynamics and saturation property of a semiconductor optical amplifier with a carrier reservoir," *IEEE Photonics Technol. Lett.* **18**, 196–198 (2006).
3. A. Kotb and C. Guo, "Theoretical demonstration of 250 Gb/s ultrafast all-optical memory using Mach–Zehnder interferometers with quantum-dot semiconductor optical amplifiers," *IEEE J. Sel. Top. Quantum Electron.* **27**, 1–7 (2021).
4. A. Kotb and C. Guo, "All-optical multifunctional AND, NOR, and XNOR logic gates using semiconductor optical amplifiers," *Phys. Scr.* **95**, 085506 (2020).
5. L. Q. Guo and M. J. Connelly, "All-optical AND gate with improved extinction ratio using signal induced nonlinearities in a bulk semiconductor optical amplifier," *Opt. Express* **14**, 2938–29433 (2006).
6. P. Singh et al., "Design, and analysis of all-optical AND, XOR and OR gates based on SOA-MZI configuration," *Opt. Laser Technol.* **66**, 35–44 (2015).
7. G. Wang, X. Yang, and W. Hu, "All-optical logic gates for 40 Gbs NRZ signals using complementary data in SOA-MZIs," *Opt. Commun.* **290**, 28–32 (2013).
8. H. Dong et al., "80 Gb/s all-optical logic AND operation using Mach–Zehnder interferometer with differential scheme," *Opt. Commun.* **265**, 79–83 (2006).
9. S. Singh, R. Kaur, and R. S. Kaler, "Photonic processing for all-optical logic gates based on semiconductor optical amplifier," *Opt. Eng.* **53**, 116102 (2014).
10. X. Zhang and N. K. Dutta, "Effects of two-photon absorption on all-optical logic operation based on quantum-dot semiconductor optical amplifiers," *J. Mod. Opt.* **65**, 166–173 (2017).
11. A. Kotb et al., "Effect of amplified spontaneous emission on semiconductor optical amplifier based all-optical logic," *Opt. Commun.* **284**, 5798–5803 (2011).

**Amer Kotb** received his PhD and MSc degrees in electronics from the University of Fayoum, Egypt in 2012 and 2006, respectively. From 2009 to 2011, he was a PhD researcher in the Department of Physics at the University of Connecticut in the USA under the supervision of Professor Niloy Dutta. From 2012 to 2015, he was an assistant professor, vice head of the Physics Department, and Chair of Students Activities at Northern Borders University in the Kingdom of Saudi Arabia. Since 2017, he has been an associate professor in the Guo Photonics Laboratory, Changchun Institute of Optics, Fine Mechanics, and Physics, Chinese Academy of Sciences, Changchun, China. Since 2018, he has been an associate professor in the Department of Physics, Faculty of Science, Fayoum University, Fayoum, Egypt.